Hindawi Publishing Corporation
Advances in Materials Science and Engineering
Volume 2013, Article ID 714868, 9 pages
http://dx.doi.org/10.1155/2013/714868

Research Article

Effect of Cooling Rate on the Microstructure of Al-Zn Alloys with Addition of Silicon as Nanocomposite

S. García-Villarreal,[1,2] A. Arizmendi-Morquecho,[1] A. Chávez-Valdez,[3] J. A. Aguilar-Martínez,[1] M. A. Esneider-Alcalá,[1] and L. Falcón-Franco[2]

[1] *Centro de Investigación en Materiales Avanzados S.C.U. Monterrey, Alianza Nte. 202, 66600 Apodaca, NL, Mexico*
[2] *Facultad de Metalurgia, UAdeC, Carr. 57, Km 4.5, 25710 Monclova, COAH, Mexico*
[3] *Katcon Institute for Innovation and Technology KIIT, Alianza Sur 200, 66629 Apodaca, NL, Mexico*

Correspondence should be addressed to A. Arizmendi-Morquecho; ana.arizmendi@cimav.edu.mx

Received 2 May 2013; Accepted 9 October 2013

Academic Editor: Peter Majewski

Al-43.5Zn-1.5Si (wt%) alloys are widely used as coatings on steel substrates. This kind of coatings is manufactured by hot-dip process, in which Si is added as solid particles or master alloy. The role of Si during formation of the coating is to control the metallurgical reactions between solid steel and liquid Al-Zn-Si alloy initially forming an AlZnFeSi intermetallic layer and next the excess of Si forms intermetallic compounds, which grows over this alloy layer, segregates into the Zn rich interdendritic regions, and solidifies as eutectic reaction product as massive particles with needle like morphology. Therefore, during the experimental procedure is very difficult to control the final morphology and distribution of the silicon phase. The acicular morphology of this phase greatly affects the mechanical properties of the alloy because it acts as stress concentrators. When the coated steel sheet is subjected to bending, the coating presents huge cracks due to the presence of silicon phase. Therefore, the aim of the paper was to propose a new methodology to control the silicon phase through its addition to Al-Zn alloy as nanocomposite and additionally determine the effect of cooling rate (between 10 and 50°Cs^{-1}) on the solidification microstructure and mechanical properties of Al-Zn alloy.

1. Introduction

Protection of steel strips against atmospheric corrosion can be obtained by coating with Al-Zn alloys. Coated steel strip panels are used for fabrication of automotive parts, electrical household appliances, and industrial constructions systems [1]. Most metallic coating fabrication processes involve bath or continuous immersion of the steel strips into liquid Al-Zn alloys at temperatures that vary according to bath composition. For example, galvanizing alloys that contain between 0.1 and 0.2 wt% Al are applied at temperatures between 450 and 460°C. In contrast, higher Al content coating alloys are applied at temperatures as high as 600°C. The quality of the coated strips is characterized by their surface appearance and their formability during sheet-metal forming processes. This property largely depends on the mechanical properties and metallurgical nature of the strip-coating interface formed as a result of the metallurgical reaction between solid steel and molten alloy.

Liquid metals are generally very aggressive against solid metals and tend to dissolve the steel during fabrication of the coating. As a result, certain alloying elements are normally added to the coating alloy to moderate its interaction with steel. For example, Al is added to pure Zn in galvanizing baths to create a submicron, continuous layer of a Fe-Al-Zn intermetallic compound that protects the steel from further attack by the liquid metal. It is evident that this protective layer must be formed as soon as the steel contacts the liquid alloy and it must not grow very thick to avoid formability problems in the coated strip. Similarly, in the case of higher Al-content Al-Zn coating alloys, Si may be added to limit the stronger and more exothermic reactions that occur as soon as the steel strips are immersed into the coating alloy. In this case, solid-liquid reactions result in the formation of

an alloy layer at the coating/substrate interface containing mainly Fe-Al and Fe-Al-Si intermetallic compounds adherent at the substrate, which affect both final thickness and steel formability [2]. But in this particular case, silicon is very difficult to control, causing the formation of large acicular particles.

Solidification of liquid coating alloy starts when the strip is air cooled at the exit of the pot. The nature of solidification of Al-Zn-Si alloys causes Zn and Si segregation to interdendritic regions and generally leads to formation of Si crystals associated with the occurrence of binary Al-Si and ternary Al-Zn-Si eutectic reactions that occur at the end of solidification. The morphology of the Si particles is irregular and acicular, and they are usually found in the intermetallic layer formed between the coating and the substrate and also in the interdendritic regions, and because of its size and distribution, commonly cracks are initiated in these particles during the bending process [3]. The heterogeneity of the microstructure and microchemistry of the coating can have important negative effects on the formability and corrosion resistance of the strips, limiting their performance during sheet-metal forming processes or service [4, 5].

Actually there are several ways of refining silicon morphology, for example, chemical composition modification (addition of elements such as Sr, Sb and Na, etc.), variations in cooling rates during processing, or the use of a subsequent heat treatment [6, 7]. Recently, it has been reported that γ-Al_2O_3 nanoparticles are ultrasonically dispersed into Al-Si melt modifying eutectic Si in hypoeutectic Al-7Si-0.3Mg alloy and refining primary Si in hypereutectic Al-20Si-4.5Cu ternary alloy during solidification process [8, 9]. However, the quantity of particles remains similar and the degree of modification can be done to a certain extent and has some limitations, especially expensive costs and in Al-Zn alloys, it can negatively influence the formation of the intermetallic layer that will result in poor adhesion to steel. Additionally, a very important processing variable that influences the formation of the microstructure during solidification is the cooling rate. This parameter controls the uniformity of the chemical composition, by limiting segregation of the microstructure. However again, silicon phase is found with acicular morphology but of smaller size. Some investigations [10–12] have been focused to determine the effect of the cooling rate on secondary dendritic arm spacing (SDAS), grain size, and the overall refinement of constituent secondary phases.

In this paper, the results of an investigation in the solidification behavior of Al-Zn-Si alloys, varying Si content in form of metallic matrix nanocomposite, is presented. The incorporation of Si to the alloy as nanoparticles was achieved making previously tablets by mechanical alloying process, in order to control the growth and distribution of Si particles in an Al-Zn matrix and subsequent incorporation into Al-Zn liquid alloys. It is intended that this microstructural modification contributes to reducing the problems associated with massive formation of intermetallic compounds, which strongly will affect the ductility and formability of the alloy and in general the mechanical properties.

Table 1: Chemical composition of the Al-Zn-Si alloys used in the present work.

Alloy	Chemical composition (wt%)					
	Al	Si	Zn	Fe	Mn	Mg
1	56.34	1.01	42.54	0.097	<0.01	<0.016
2	55.61	1.22	43.06	0.091	<0.01	<0.01
3	55.68	1.53	42.69	0.097	<0.01	<0.01
4	54.26	1.81	43.83	0.096	<0.01	<0.01

2. Materials and Methods

Al-43.5Zn-1.5Si (wt%) nanocomposites were manufactured by mechanical alloying using a SPEX mill Model 8000M. In this process, the starting material was 55Al-Zn (wt%) alloy, which was previously melted, solidified, and cut in a 1 mm burr of average size. Then, Si as nanoparticles, with average particle size of 50 nm (from Sky Spring Nanomaterials), was manually incorporated in the Al-Zn alloy. Al-Zn alloy and Si nanoparticles (10 g) and steel balls (40 g) were charged into a stainless steel container with argon atmosphere. Also, 1 vol% of ethanol was added as process control agent to prevent cold welding. Milling time was maintained constant during 10 hours. This procedure was performed repeatedly to obtain sufficient nanocomposite powder. From the product in form of powder, tablets were obtained by hot pressing, using a 4122 Carver hydraulic press with a load of 10.5 tons during 10 minutes, which in a subsequent process were incorporated to the liquid alloy allowing easy disintegration. The density of the tablets was determined with a pycnometer of helium gas obtaining values of 3.25 ± 0.07 g/cc. Porosity of the composite was measured through image analysis resulting in 4.3% ± 0.5. A good quantity of nanocomposite was manufactured in order to produce four Al-Zn-Si alloys varying silicon content between 1.0 and 1.8 wt%, as can be seen in Table 1. Zn content in four alloys remains within 42–43 wt% and Al content remains between 54 and 56 wt%. The main impurity in all four alloys was Fe that remained constant at a level of ~0.1 wt%. A solidification study was developed by thermal analysis experiments over a range of different cooling rates (i.e., different solidification times) between 5 and 50°Cs^{-1}. The various cooling rates were achieved by using different cooling media in the experimental apparatus showed in Figure 1. Microstructural analysis of the milling nanocomposite was characterized by TEM (STEM mode) with a JEOL JEM-2200FS HRTEM with spherical aberration corrector and acceleration of 200 kV. A high-angle annular dark field (HAADF) was used in the STEM mode for acquiring images with chemical information (Z-contrast). The elemental analysis was performed with the EDXS technique (model Oxford Instruments Sight Inca). The solidified samples were sectioned longitudinally and prepared by conventional metallographic techniques with the aim to characterize the solidification microstructures from different cooling conditions. Image analysis technique was used to measure SDAS using the line interception method taking at least 30 measurements at different locations on the surface of the samples. The corresponding cooling rates

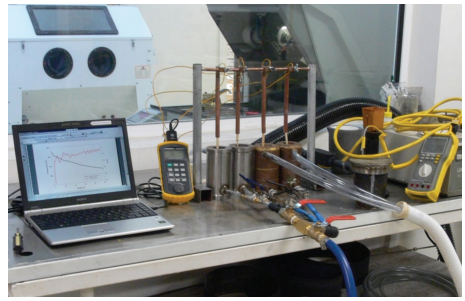

Figure 1: Experimental apparatus for thermal analysis and solidification process.

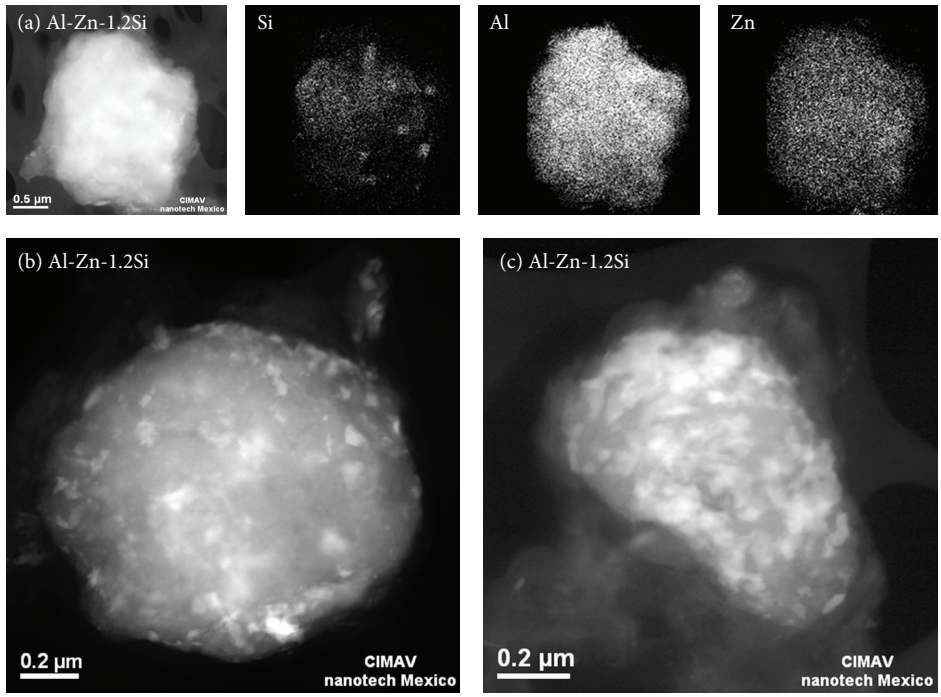

Figure 2: (a) Elemental distribution maps of Al-Zn-1.2Si (wt%) nanocomposite; ((b) and (c)) dark field Z-contrast images obtained from STEM of Al-Zn-Si nanocomposite.

were determined directly from the experimental cooling curves. Finally Vickers microhardness (HV) was evaluated in a Micro-Hardness Tester (Clemex MMT-X7), using an indentation time of 10 s and a maximum load of 10 g. 10 indentations were made randomly on surface of samples that were prepared by conventional metallographic techniques and a average of them was calculated. Tensile strength of alloys was determined issuing the specimens having a gage of 6.35 mm thickness and 6.35 mm width, with a gage length of 25.4 mm at cross head speed of 0.3 mm s^{-1}. These mechanical tests were evaluated in a machine Shimadzu (AG-X 100 KN).

3. Results and Discussion

Figure 2 shows EDXS maps with the distribution of Si, Al, and Zn in the microstructures of Al-Zn-1.2Si (wt%) nanocomposites obtained with 10 h of mechanical milling. EDXS allowed the identification of Si particles associated with the Al-Zn matrix after 10 h milling showing an average size of ~50 nm. Si appears distributed in the metal matrix and Al and Zn as homogeneous solid solution. Additionally, this figure shows dark field (Z-contrast) images obtained from STEM mode of Al-Zn-Si nanocomposites. The Z-contrast image is sensitive to the average atomic number; therefore, Zn appears more brilliant than Al due to its atomic number [13]. Al rich phase appears in gray contrast while the Zn rich phase appears in white contrast. On the other hand, due to the atomic number of Si and the amount added in the nanocomposite, this element was no detected through this technique. However, it is present in the particles according to the EDXS results.

Figures 3(a) and 3(b) show bright field high-resolution images from Al-Zn nanocomposites with 1.2 (wt%) of Si nanoparticles. Obscure point of the indicated area corresponds to Si nanoparticles with a size of ~100 nm, which were associated with Al-Zn metallic matrix after 10 h of milling.

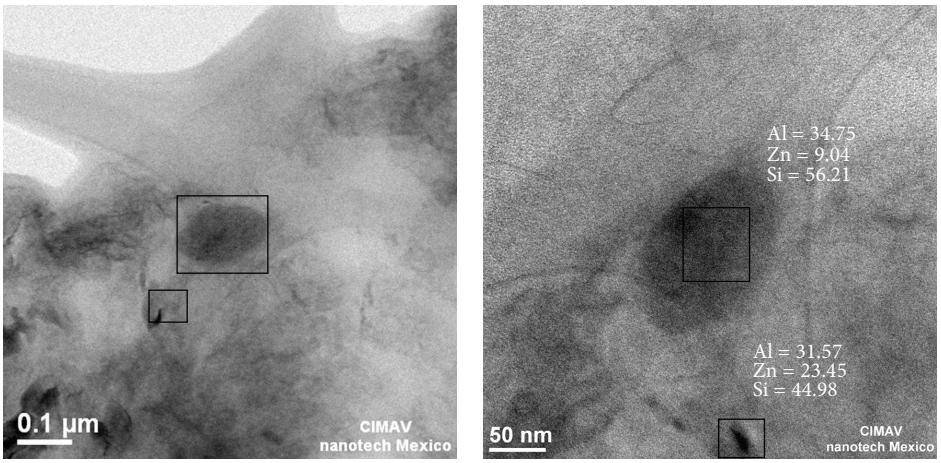

(a) (b)

Figure 3: ((a) and (b)) Bright field high-resolution TEM images and EDXS results (wt%) of Al-Zn-1.2Si nanocomposites.

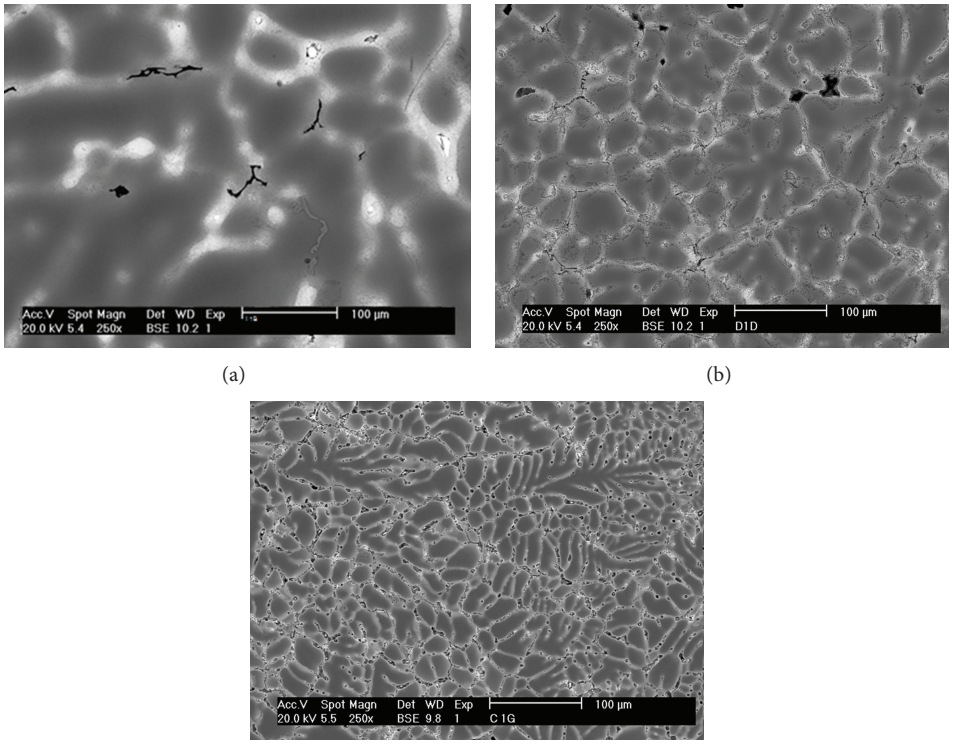

(a) (b)

(c)

Figure 4: SEM-backscattered electron images illustrating the effect of cooling rate on the solidification microstructure of Al-Zn-Si alloys with 1.5Si wt%: (a) 11.7°Cs^{-1}, (b) 31.5°Cs^{-1}, and (c) 50.1°Cs^{-1}.

As it can be seen in high-resolution images, Al and Zn rich phases are present as solid solution. This observation was supported by EDXS microanalysis indicated in Figure 3(b) from different areas; also silicon appears dissolved in aluminum phase.

On the other hand, Figures 4(a) to 4(c) present a series of backscattered electron images illustrating the effect of cooling rate on the overall solidification microstructure of conventional Al-Zn-Si alloy with 1.5 wt% Si added. In general, the microstructure consists of a two-dimensional dendritic network surrounded by interdendritic channels. As can be seen, Figure 4(a) shows that with slower cooling rate, the secondary dendrite size (SDAS) is larger. In contrast, in Figures 4(b) and 4(c) will be observed as increasing the cooling rate decreases the SDAS; therefore, increasing the cooling rate causes significant and progressive refinement of the microstructure which is associated with decreasing time available for dendrite growth and solute redistribution.

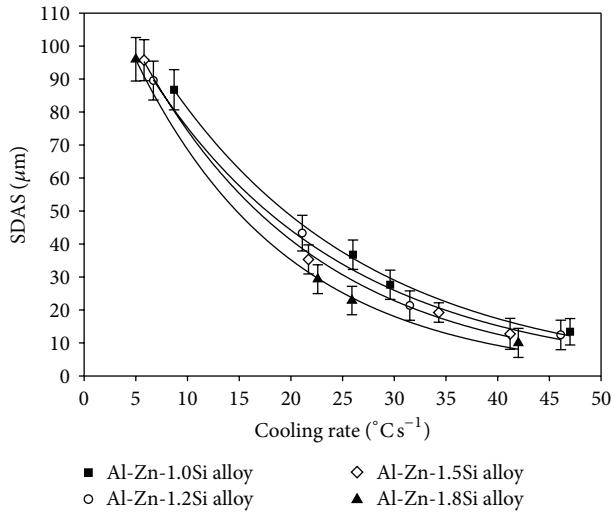

FIGURE 5: Effect of cooling rate and Si content on SDAS of Al-Zn-Si alloys.

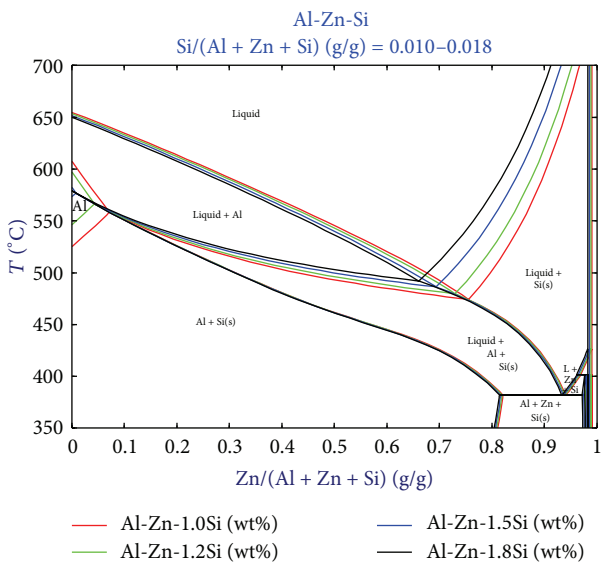

FIGURE 6: Effect of silicon content on Al-Zn phase diagram obtained from FactSage Software.

Accordingly, the morphology and distribution of second phase particles formed within interdendritic regions also change dramatically. However, regardless of the cooling rate, silicon phase remains as eutectic constituent with acicular morphology.

A plot illustrating a relationship between SDAS and cooling rate is shown in Figure 5 for four alloys with Si content added as nanocomposite between 1.00 and 1.81 wt%. As can be seen, in general, values of SDAS decrease faster at cooling rates below 20°Cs^{-1}. This effect appears to be more important for alloys with higher Si content. With higher cooling rates, the segregation of silicon particles is limited resulting in smaller values of SDAS. In contrast, slow cooling rates causes more time available for the silicon segregation

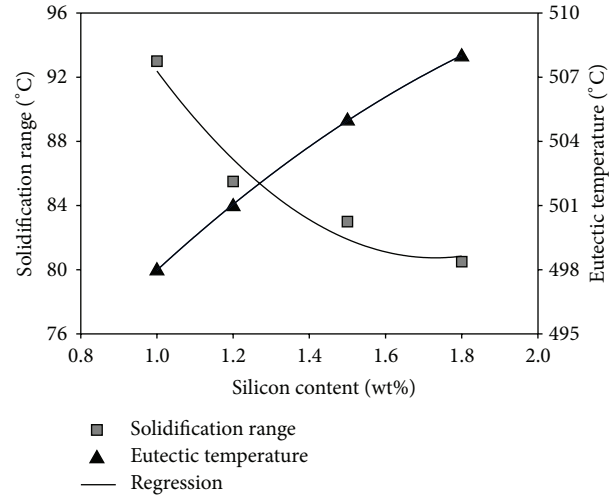

FIGURE 7: Effect of silicon content on the solidification range in Al-Zn alloys.

to the interdendritic regions and therefore the particles have more time to grow and affecting the SDAS values. However differences in SDAS with the different silicon contents can be an effect of solidification range, as it can be seen in the Al-Zn-Si isopleths in equilibrium of Figure 6. According to the trend showed in Figure 7, the solidification range (T_{solidus}–T_{liquidus}) decreases with the increase in Si content. Nonetheless, the starting temperature of the eutectic reaction increases with Si content. Because of this, temperature range for growth of primary dendrites is lower with higher Si contents and therefore the SDAS is smaller, but in the microstructure more particles of Si with eutectic composition will be found. This relationship between SDAS and cooling rate for Al-Zn-Si alloy has practical significance, because it serves to control the refinement of final microstructure.

Detailed examination of the solidification microstructure under the SEM confirmed that, apart from its apparent effect on the cooling rate dependence of SDAS, the most significant effect of Si was on the morphology of particles formed within interdendritic regions. As it can be seen in Figure 8, a comparison of the microstructures obtained by SEM of Al-Zn-Si alloys solidified at low and high cooling rate is presented. From the overall microstructure, silicon phase was selected to analyze their morphology. As it can be seen, morphology of eutectic particles was found to vary with cooling rate. Silicon particles greater than 20 μm were found in conventional alloys; in these samples, silicon phase has an acicular morphology when low and high cooling rate are used. On the other hand, when silicon is added as nanocomposite to Al-Zn liquid alloy, the final microstructure consists of Al primary solid solution dendrites, Zn-Al interdendritic regions and Si-rich eutectic particles. However in this case, silicon phase appears only with blocky morphology, reaching as maximum 3 μm in length when low cooling rate is used, and 1 μm or less when high cooling rate is used. Table 2 shows the results of EDXS microanalysis of the main phases in Al-Zn-1.5Si (wt%) alloy with addition of silicon as nanocomposite solidified at different cooling rates. EDXS microanalysis showed that

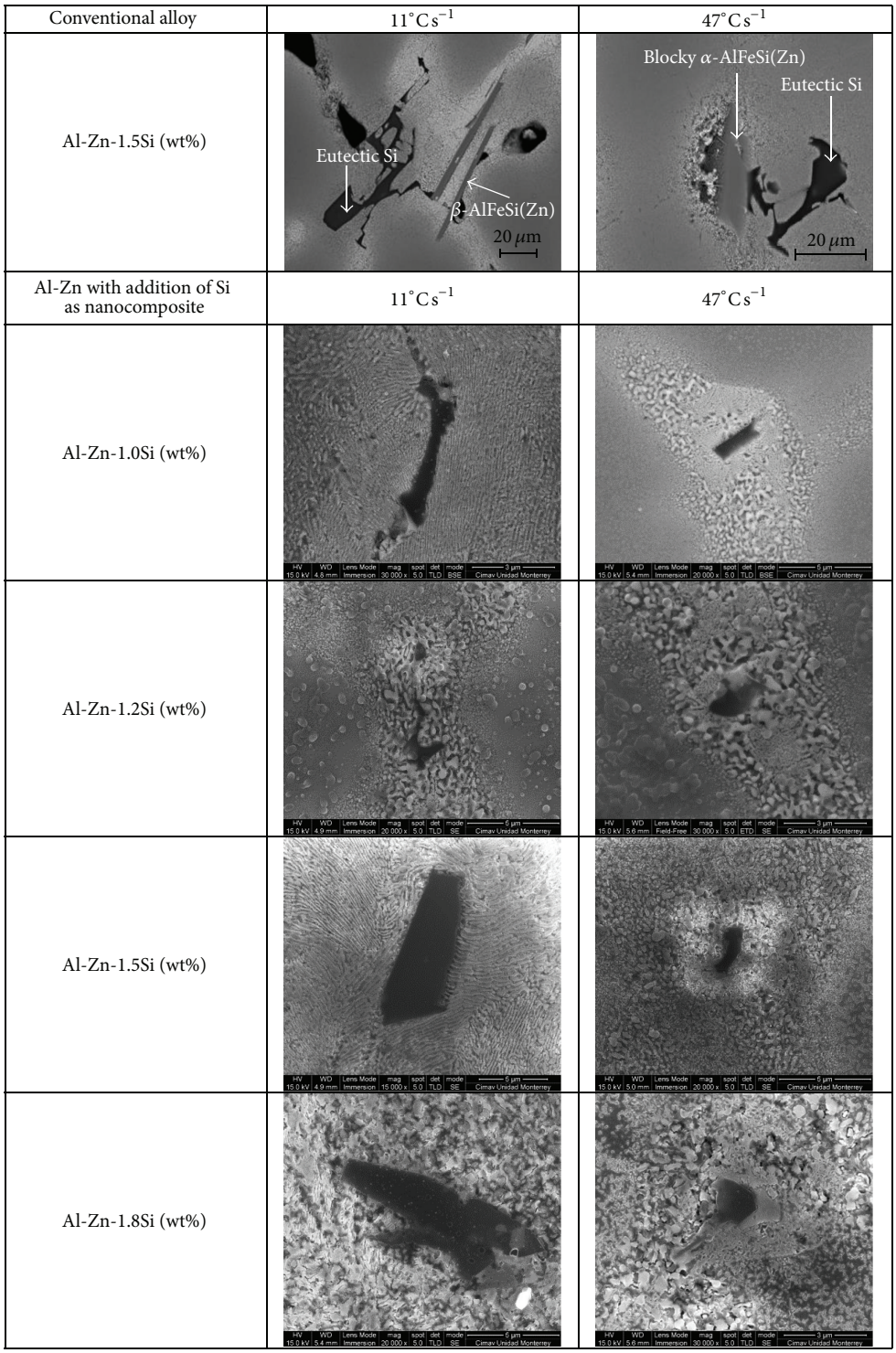

Figure 8: Electron images illustrating a comparison of the morphology of silicon particles in Al-Zn-Si alloys solidified at low and high cooling rate.

silicon is present only in the dark particles, as product of eutectic solidification. These observations suggest that local chemical composition, cooling rate, and the form to add silicon element are the controlling factors that determine the nature and morphology (size and shape) of the phases that form during solidification of these materials. However, if the Si concentration in the liquid is not carefully controlled, the quantity and morphology of particles formed as a result of Si excess may have adverse effects on mechanical properties of the alloy. These particles can act as stress concentrators and become preferential sites for crack nucleation during forming operations [4].

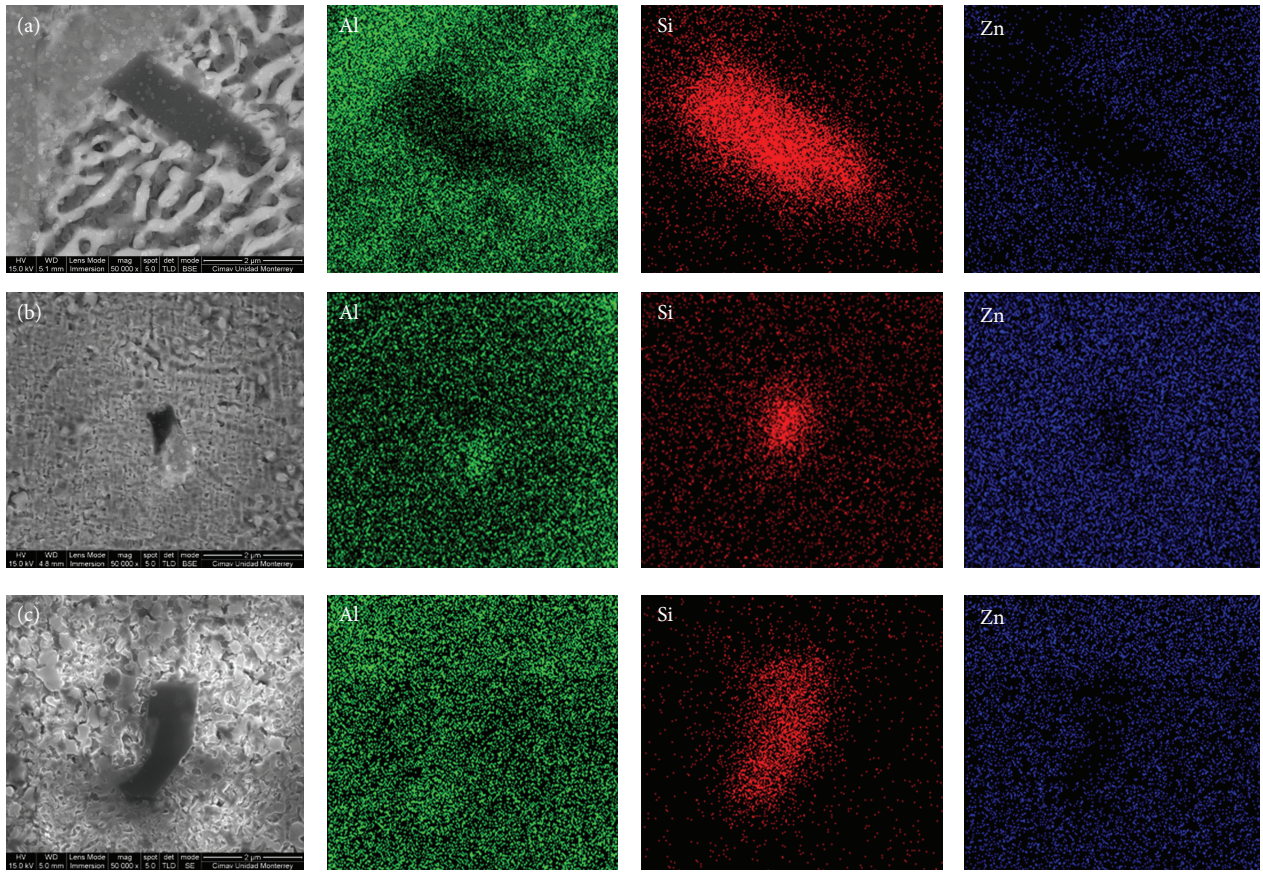

Figure 9: Maps of Al, Si, and Zn element distribution observed in the microstructures of Al-Zn-1.0Si alloy (wt%) at cooling rates of (a) 11.7°Cs^{-1}, (b) 29.6°Cs^{-1}, and (c) 47.0°Cs^{-1}.

Table 2: EDXS microanalysis of the Al-Zn-1.5Si (wt%) modified alloy solidified at different cooling rates.

Phase morphology	Sample condition		Average chemical composition (wt%)		
	dT/dt (°C s^{-1})	Si (wt%)	Al	Zn	Si
Dendritic region	11.7	1.53	80.7	19.3	—
	31.5	1.53	78.0	22.0	—
	50.1	1.53	85.0	15.0	—
Interdendritic region	11.7	1.53	10.3	89.7	—
	31.5	1.53	23.8	76.2	—
	50.1	1.53	20.1	79.9	—
Al-Zn-Si Eutectic (blocky)	11.7	1.53	13.5	31.6	54.9
	31.5	1.53	20.8	23.4	55.8
	50.1	1.53	8.1	34.5	57.4

To obtain a general view of elemental distributions in the microstructure of Al-Zn-Si alloy modified with addition of silicon as nanocomposite, characteristic X-ray maps of some specific areas of the microstructure were obtained by EDXS. Figure 9 illustrates Al, Si, and Zn distributions in the microstructures of Al-Zn-1.0Si (wt%) alloy solidified at cooling rates of 11.7, 29.6, and 47.0°Cs^{-1}. As can be seen, Si is clearly associated only with secondary phase particles formed within interdendritic regions. This observation suggests that, independent of cooling rate, these elements exhibit a strong interdendritic segregation tendency. In contrast, Zn appears to be rather uniformly distributed over the whole microstructure. A similar effect is observed for Al. According to the microstructural observations and neglecting the Fe content, a proposed mechanism for the solidification of Al-43.5Zn-1.5Si (wt%) alloy in equilibrium is as follows. At 555.58°C a dendritic solid solution rich in Al begins to form, next at 505.36°C occurs the eutectic reaction between Al + Si, the solidification ends at 472.96°C. On the other hand, when high cooling rate is used, the solidification occurs out of equilibrium (Scheil cooling). In this case, the mechanism is as follows. At 555.58°C, a dendritic solid solution rich in Al begins to form, next at 504.82°C, the formation of dendrites segregate silicon and at this temperature, binary eutectic reaction occurs between Al + Si, the decreases of Si and Zn solubility in the solid solute cause enrichment of these elements in the remaining interdendritic liquid, and at 381.59°C the last liquid solidifies as ternary eutectic Al + Zn + Si.

Finally, the variation of hardness and tensile strength regarding silicon content of Al-Zn alloys is shown in

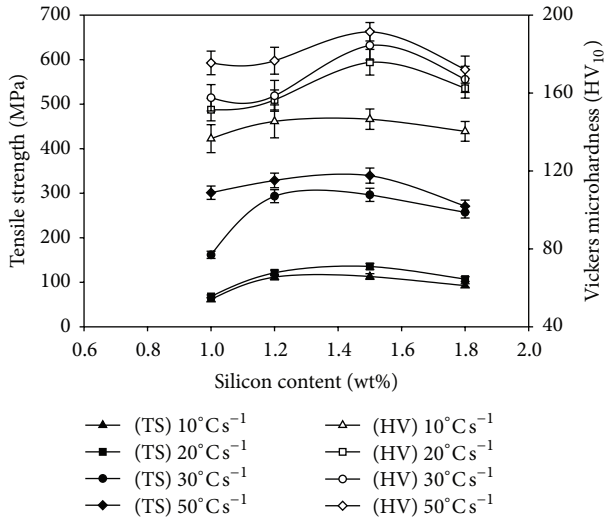

Figure 10: Effect of Si content on the microhardness and tensile strength of Al-Zn alloys with different cooling rates.

Figure 10. As can be seen, hardness and tensile strength have similar tendencies and mechanical properties are higher with the increment on cooling rate. This effect can be associated directly with the smaller values of SDAS and more homogeneous distributions of smaller grain size observed in samples solidified at faster cooling rates. When low cooling rate is used, the Si content has no significant effect on the mechanical properties of the alloy. However, it is noteworthy that, hardness and tensile strength reach a maximum at 1.5 wt% silicon. When Si content is increased beyond 1.5 wt%, fast cooling rates cause a sudden decrease in mechanical properties. At fast cooling rates, the observed behavior can be explained in terms of the effect of Si concentration on the solidification pattern of the final interdendritic liquid. As shown earlier, Si segregates strongly to interdendritic regions. Neglecting the effect of Zn and assuming that Si is fully segregated to the interdendritic liquid, final eutectic solidification takes place in alloys with Si > 1.5 wt%. When solidification takes place slowly, formation of relatively large eutectic Si particles contributes significantly to the average hardness of the material. In contrast, when Si < 1.5 wt%, solidification takes place by continuous formation of Al-rich dendrites with progressively higher Si concentrations. However, in this case, solidification ends before the Si concentration required for eutectic solidification is reached. As a result, fast cooling promotes supersaturation of the primary Al phase and the hardness increases as the Si concentration increases. Evidently, this effect is stronger at higher Si concentrations. For alloys with Si > 1.5 wt% solidified at fast cooling rates, eutectic solidification decreases the amount of Si available for supersaturation of the primary dendrites and, as a result, the hardness and tensile strength values decrease suddenly.

4. Conclusions

Al-Zn-Si nanocomposites have been produced by incorporation of silicon nanoparticles into Al-Zn metal matrix by mechanical alloying. In this work, it was possible to change the size, morphology, and distribution of Si in the final microstructure by varying the form of addition to the Al-Zn matrix as nanocomposite. The primary Si particles are refined from the acicular shape to the polygon or blocky shape, and their edges and corners were smoother. This methodology has a beneficial effect on the final microstructure and mechanical properties of Al-Zn-Si alloys. Si distributed as nanocomposite during solidification segregates to the interdendritic regions forming only small particles with blocky morphology and results in aluminum and zinc rich phases without silicon impurities. The experimental results presented in this paper demonstrated that increasing the cooling rate during solidification of Al-Zn-Si alloys causes general refinement of microstructure. The microhardness and tensile strength of the based Al-Zn-Si alloys increased with increasing silicon content up to 1.5 wt%, above which they decreased as the silicon content increased further. The investigated nanocomposites have potential applications for manufacturing in the future formable coatings on steel sheets.

Acknowledgments

S. García-Villarreal gratefully acknowledges the financial support from the Consejo Nacional de Ciencia y Tecnología (Conacyt-México) for the doctoral grant (Scholarship No. 228136). The authors thank N. Pineda and L. Orrantia for their technical assistance.

References

[1] A. Costa e Silva, R. R. Avillez, and K. Marquez, "A preliminary assessment of the Zn-rich Corner of Al-Fe-Zn system and its implications in Steel coating," *Zeitschrift für Metallkunde*, vol. 90, pp. 38–43, 1999.

[2] J. H. Selverian, A. R. Marder, and M. R. Notis, "The reaction between solid iron and liquid Al-Zn baths," *Metallurgical Transactions A*, vol. 19, no. 5, pp. 1193–1203, 1988.

[3] A. M. Arizmendi, A. R. Salinas, E. V. Nava, and R. C. Garza, "Microstructure of Al-Zn-Si Coatings on Steel Substrates," *Materials Science Forum*, vol. 442, pp. 43–48, 2003.

[4] J. H. Selverian, A. R. Marder, and M. R. Notis, "The effects of silicon on the reaction between solid iron and liquid 55 wt pct Al-Zn baths," *Metallurgical Transactions A*, vol. 20, no. 3, pp. 543–555, 1989.

[5] H. J. Cleary, "The microstructure and corrosion resistance of 55%Al-Zn coatings on sheet steel," in *Corrosion, Microstructure and Metallography*, D. O. Northwood, Ed., vol. 12 of *Microstructure Science*, pp. 103–113, ASM International, 1994.

[6] S. D. McDonald, K. Nogita, and A. K. Dahle, "Eutectic nucleation in Al-Si alloys," *Acta Materialia*, vol. 52, no. 14, pp. 4273–4280, 2004.

[7] A. K. Dahle, K. Nogita, J. W. Zindel, S. D. McDonald, and L. M. Hogan, "Eutectic nucleation and growth in hypoeutectic Al-Si alloys at different strontium levels," *Metallurgical and Materials Transactions A*, vol. 32, no. 4, pp. 949–960, 2001.

[8] H. Choi, M. Jones, H. Konishi, and X. Li, "Effect of combined addition of Cu and aluminum oxide nanoparticles on mechanical properties and microstructure of Al-7Si-0.3Mg

alloy," *Metallurgical and Materials Transactions A*, vol. 43, no. 2, pp. 738–746, 2012.

[9] H. Choi and X. Li, "Refinement of primary Si and modification of eutectic Si for enhanced ductility of hypereutectic Al-20Si-4.5Cu alloy with addition of Al_2O_3 nanoparticles," *Journal of Materials Science*, vol. 47, no. 7, pp. 3096–3102, 2012.

[10] R. MacKay, M. Djurdjevic, and J.H. Sokolowski, "The effect of cooling rate on the fraction solid of the metallurgical reaction in the 319 alloy," *AFS Transactions*, vol. 108, pp. 521–530, 2000.

[11] A. K. Dahle, J. E. Hutt, Y. C. Lee, and D. H. StJohn, "Grain formation in hypoeutectic Al-Si alloys," in *Proceedings of the 103rd AFS Casting Congress*, pp. 265–270, St. Louis, Mo, USA, March 1999.

[12] P. Kumar and J. L. Gaindhar, "DAS, solidification time and mechanical properties of Al-11%Si alloy V processed castings," *AFS Transactions*, vol. 9, pp. 635–638, 1997.

[13] S. J. Pennycook and L. A. Boatner, "Chemically sensitive structure-imaging with a scanning transmission electron microscope," *Nature*, vol. 336, no. 6199, pp. 565–567, 1988.